



Cohesive modeling of fatigue crack retardation in polymers: Crack closure effect

Spandan Maiti, Philippe H. Geubelle *

*Department of Aerospace Engineering and Beckman Institute of Science and Technology, University of Illinois
at Urbana-Champaign, 306 Talbot Lab, 104 S Wright Street, Urbana, IL 61801, USA*

Received 16 December 2004; received in revised form 15 June 2005; accepted 5 July 2005

Available online 12 September 2005

Abstract

A numerical model of fatigue crack growth retardation in polymers induced by artificial crack closure is proposed. The approach relies on the combination of cohesive modeling and a contact algorithm incorporated in the wake of the advancing crack to account for the effect of the introduced wedge. Numerical results are compared with existing experimental observations, showing the ability of the cohesive model to capture the key features of wedge-induced crack retardation. A study is conducted to quantify the effects of relevant parameters such as applied load levels, wedge distance to the crack tip and wedge stiffness. The model is also discussed in the context of self-healing polymers [White SR, Sottos NR, Moore J, Geubelle PH, Kessler M, Brown E, et al. Autonomic healing of polymer composites. *Nature* 2001;409:794–7], where the wedging effect is associated with the polymerization of the healing agent.

© 2005 Elsevier Ltd. All rights reserved.

Keywords: Fatigue crack retardation; Artificial crack closure; Wedge; Contact; Cohesive finite element; Polymeric materials

1. Introduction

Fatigue is often a key failure mechanism in structural components and substantial efforts have been made to propose and investigate different mechanisms for the retardation of fatigue crack propagation. One of these mechanisms relies on the shielding of the crack tip [14], which reduces the effective stress range at the crack tip through the crack closure effect. The closure produced by the plastically deformed material left in the wake of a propagating fatigue crack in metals and its effect on the crack growth rate have first been observed by Elber [7]. Later, it was demonstrated that the crack closure effect can also be achieved by

* Corresponding author. Tel.: +1 217 244 7648; fax: +1 217 244 0720.
E-mail address: geubelle@uiuc.edu (P.H. Geubelle).

Nomenclature

α, β	material parameters for fatigue cohesive model
b_0	uncracked length of the beam
da/dN	crack advance per cycle
C	intercept of the Paris curve
Δ	displacement jump vector
ΔU	displacement correction vector
Δ_{applied}	applied displacement
Δ_n	crack opening displacement vector
Δ_n^*	thickness of inserted wedge
Δ_{nc}	critical opening displacement jump
E	Young's modulus
Γ_c	cohesive surface
g	gap function
G_{Ic}	fracture toughness
\mathbf{K}_b	partition of stiffness matrix of beam corresponding to contacting nodes
\mathbf{K}_{coh}	cohesive stiffness matrix
\mathbf{K}_{vol}	volumetric tangent stiffness matrix
\mathbf{K}_w	partition of stiffness matrix of wedge corresponding to contacting nodes
k_{coh}	cohesive stiffness
K_{Ic}	critical stress intensity factor in mode I
K_{min}	minimum stress intensity factor
K_{max}	maximum stress intensity factor
ΔK	applied loading range
ΔK_{eff}	effective stress intensity factor range
N_f	number of loading cycles since onset of failure
p	contact force
R	load ratio
\mathbf{R}	external load vector
σ_{max}	tensile cohesive failure strength
\mathcal{S}	damage parameter
$\mathcal{S}_{\text{init}}$	initial value of damage parameter
\mathcal{S}_p	previous value of damage parameter
\mathbf{T}	cohesive traction vector
T_n	normal component of cohesive traction
\mathbf{U}	displacement vector
W	wedge equivalent stiffness

oxide [22], roughness [9,15], phase transformation [10], or fluid pressure-induced closure [8]. Kitagawa and co-workers [11] first demonstrated artificial crack closure by inserting a wedge in the wake of the crack. This method of fatigue crack retardation was subsequently studied in [17,19–21,23,24]. All the aforementioned mechanisms slow down fatigue crack growth by increasing the minimum stress intensity factor K_{min} , thereby reducing the effective stress intensity factor range ΔK_{eff} experienced by the crack tip. Sharp and co-workers [17] also showed that an adhesive wedge is further capable of fatigue crack retardation by bonding with the crack faces, further reducing the maximum stress intensity factor K_{max} .

All the experimental observations contained in the references listed above have been obtained on metallic specimens subjected to a constant stress intensity factor range. Due to their intrinsic brittleness, most polymeric materials do not experience plasticity-induced crack closure. Furthermore, many of the other artificial crack closure mechanisms outlined so far are not applicable for this class of material. The only practical ways to achieve fatigue crack retardation in polymers through crack closure may be the artificial infiltration of a viscous fluid or a solid wedge in the wake of the crack. One of the very few reported experimental observations of the effect of a wedge on the propagation of a fatigue crack in polymeric materials can be found in [2], where a study of fatigue crack propagation in epoxy to observe the effect of autonomous healing on the retardation of the fatigue crack growth has been undertaken. This study employs the self-healing technique developed by White and co-workers [25] for quasi-static loading case and extends that concept for polymeric systems under cyclic loading. Healing is achieved by a special material system containing a monomer (dicyclopentadiene or DCPD) filled spherical particles embedded in the polymer matrix. The matrix also contains a Ruthenium-based catalyst which initiates the polymerization of the monomer stored in the microspheres. When the advancing crack ruptures a sphere, the monomer is released in the matrix filling up the wake of the crack and subsequently polymerizes after coming into contact with the catalyst. DCPD released in the wake is initially in liquid form. After reaching the gelation point, it adheres to the crack faces before finally solidifying to act as a wedge in the wake of the crack. The phase change of the filling material (DCPD) is quite complex and depends on its cure kinetics with the associated change in mechanical strength and fracture properties. If the rate of crack advance is small enough and/or a rest period is provided, sufficient solidification of the infiltrated material can be achieved and the dominant mechanism of the fatigue crack retardation in this particular situation is the crack closure due to wedge effect. This effect is therefore the topic of the analytical study presented hereafter.

Various theoretical models have been developed to explain and predict the crack retardation and arrest due to crack closure [23,27,18]. Ur-Rehman and Thomason [23] modeled the wedge as a rigid body of uniform thickness in the wake of the crack. Shin and Cai [18] argued that the wedge may not behave rigidly and used an elastic–perfectly plastic material model for the wedge instead. As they investigated the crack propagation behavior of metallic alloys infiltrated with polymeric wedges, they assumed all the deformations to be on the wedge only. They found that, above a certain value, the Young's modulus and yield strength of the wedge does not affect the crack retardation. Yanyan and co-workers [27] formulated a model for an equivalent crack opening load for the special case of three-point-bending specimens. All these models have however limiting assumptions on the geometry of the specimen, the loading conditions, the deformation localization or the path of crack propagation. No model has been developed yet to study the fatigue crack retardation using artificial wedges in a general setup.

The approach adopted in this work relies on cohesive modeling, which has been recognized as a powerful method to simulate in unified setup a wide variety of crack propagation events under complex geometric and loading situations. Recently, this technique has been successfully employed to study the crack propagation under cyclic loading [12,13,16,26]. In this paper, we present a numerical model based on the cohesive finite element technique to study the effect of an infiltrated wedge on the fatigue crack propagation in brittle polymers. As mentioned earlier, this class of materials shows no or negligible plasticity to induce crack closure. The dominant mechanism responsible for the fatigue crack propagation is thus the infiltrated wedge in the wake of a crack. Crack closure in the wake of the crack is modeled by a contact enforcement technique based on link elements. Although the model developed in this paper is general and does not assume the wedge to be rigid, we focus our attention in most applications on the case of a rigid wedge. The effects of the wedge thickness and infiltration techniques, i.e., the placement of the wedge behind the crack tip, are investigated, and a reference is made to the crack retardation mechanism in self-healing polymers [2] where the wake of the crack is bridged continuously as the crack advances.

We start this paper with a brief review of the cohesive model used to simulate fatigue crack propagation in polymers. Next, we discuss in Section 3 the model used to take into account the presence of a wedge in

the wake of a crack. Results from a detailed parametric study are presented in Section 4 together with comparisons with experimental observations reported in the literature.

2. Cohesive modeling of fatigue crack growth

As mentioned in the previous section, cohesive models have recently appeared for fatigue crack growth in metals [4–6,13], along interfaces [16] and in quasi-brittle materials [26]. The model that serves as the foundation for the present wedge-induced crack retardation study is the phenomenological cohesive model recently developed by the authors, which is particularly suitable for polymers with higher fatigue sensitivity [12]. For the sake of completeness, we summarize here the basic features of this model.

The cohesive model starts with a bi-linear, rate-independent, damage-dependent irreversible failure law between the cohesive traction vector \mathbf{T} and the displacement jump vector Δ acting across the cohesive surfaces Γ_c . In the tensile (mode I) case, which is the focus of the work presented hereafter, this cohesive model takes the simple form

$$T_n = \frac{\mathcal{S}}{1 - \mathcal{S}} \frac{\Delta_n}{\Delta_{nc}} \frac{\sigma_{\max}}{\mathcal{S}_{\text{init}}} = k_{\text{coh}} \Delta_n, \quad (1)$$

where T_n and Δ_n respectively denote the normal component of the cohesive traction and crack opening displacement vectors, σ_{\max} is the tensile cohesive failure strength, and Δ_{nc} the critical value of the opening displacement jump beyond which complete failure is assumed. The corresponding fracture toughness G_{Ic} is the area under the traction-separation curve and is given by

$$G_{Ic} = \frac{1}{2} \sigma_{\max} \Delta_{nc}.$$

The evolution of the damage process is quantified by the monotonically decreasing damage parameter \mathcal{S} defined as

$$\mathcal{S} = \min(\mathcal{S}_p, \langle 1 - \Delta_n / \Delta_{nc} \rangle), \quad (2)$$

where $\langle a \rangle = a$ if $a > 0$ and $= 0$ otherwise, and \mathcal{S}_p denotes the previously achieved \mathcal{S} value. $\mathcal{S}_{\text{init}}$ denotes the initial value of this quantity which is set at approximately 1 (0.98 in this work) and controls the slope of the rising part of the cohesive traction-separation law. Due to its monotonically decreasing nature, \mathcal{S} represents the current damage state and prevents healing of the cohesive elements in the event of unloading and subsequent reloading. Also, the cohesive stiffness k_{coh} in (1) reduces monotonically as Δ_n increases and becomes zero when the critical opening displacement jump Δ_{nc} has been achieved.

The fatigue-induced irreversibility is accounted for by specifying an irreversible unloading-reloading path through the rate of change of cohesive stiffness \dot{k}_{coh} :

$$\dot{k}_{\text{coh}} = \begin{cases} -\frac{1}{\alpha} N_f^{-\beta} k_{\text{coh}} \dot{\Delta}_n & \text{if } \dot{\Delta}_n \geq 0, \\ 0 & \text{if } \dot{\Delta}_n \leq 0, \end{cases} \quad (3)$$

where N_f denotes the number of loading cycle experienced by the material point since the onset of failure, i.e., at the time the cohesive traction T_n first reached the failure strength σ_{\max} , α and β are material parameters describing the fatigue-induced degradation of cohesive properties, and $\dot{\Delta}_n$ is the rate of change of the normal separation. The cohesive law is schematically presented in Fig. 1. As shown in [12], the parameters α and β determine the intercept and slope of the Paris fatigue curve (i.e., log–log plot of crack advance per cycle, da/dN , vs. applied loading range, ΔK). A detailed discussion of this cohesive model alongwith its effect on the upper and lower thresholds of fatigue crack growth can also be found in [12]. As shown there,

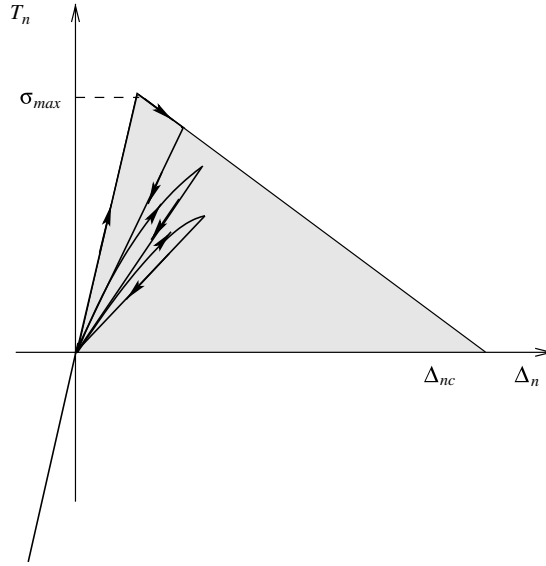


Fig. 1. Schematic representation of the progressive degradation of the cohesive properties during sub-critical unloading and reloading events due to fatigue loading. The shaded area corresponds to the monotonic fracture toughness G_{Ic} .

the existence of a lower fatigue threshold is associated with the initial value \mathcal{S}_{init} of the damage parameter \mathcal{S} .

The fatigue cohesive model is implemented in a finite element scheme combining volumetric elements used to capture the bulk response of the material and cohesive elements used to model the fatigue process. A quasi-implicit load stepping scheme is used in this investigation to form the equations of equilibrium. The tangent stiffness matrix arising from the volumetric elements, \mathbf{K}_v , and the cohesive component of the stiffness matrix, \mathbf{K}_{coh} , are updated at each load step based on the displacements (and corresponding displacement jumps) achieved at the previous loading step. The equations of equilibrium for a load step n can be written as

$$[\mathbf{K}_{coh}(\mathbf{U}_{n-1}) + \mathbf{K}_v(\mathbf{U}_{n-1})]\mathbf{U}_n = \mathbf{R}_n, \quad (4)$$

where \mathbf{R}_n is the external load vector at the n th load step. Denoting the sum of $\mathbf{K}_{coh}(\mathbf{U}_{n-1})$ and $\mathbf{K}_v(\mathbf{U}_{n-1})$ by \mathbf{K}_n for simplicity, and noting that $\mathbf{U}_n = \mathbf{U}_{n-1} + d\mathbf{U}_n$, where $d\mathbf{U}_n$ is the increment in loading for the n th time step, we can restate (4) as

$$\mathbf{K}_n d\mathbf{U}_n = \mathbf{R}_n - \mathbf{K}_n \mathbf{U}_{n-1}. \quad (5)$$

For linear volumetric response, the tangent stiffness matrix \mathbf{K}_v remains constant through all the loading steps and needs to be calculated only once.

Fig. 2 presents a comparison between experimental fatigue crack propagation data in epoxy [1] and simulation results obtained with the fatigue cohesive model described by (1)–(3). The experimental values of the crack growth rate da/dN were obtained with a tapered cantilever beam specimen made of neat EPON 828 epoxy resin with 12 pph Ancamine DETA (diethylenetriamine) curing agent subjected to a range of cyclic loading conditions. In the simulations, the maximum amplitude of the applied displacement $\Delta_{applied}$ was taken to be 1.8 mm resulting in an initial value of the maximum stress intensity factor $0.6 \text{ MPa} \sqrt{\text{m}}$. The load ratio R , the ratio of minimum to maximum applied load, was taken to be 0.1. In the example shown in Fig. 2, the uncracked length of the beam $b_0 = 100 \text{ mm}$, the Young's modulus $E = 3.4 \text{ GPa}$, the

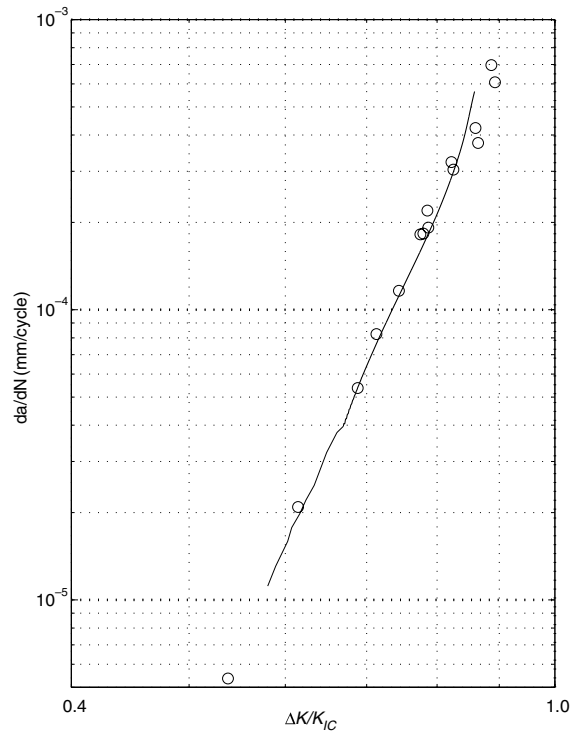


Fig. 2. Comparison between experimental (symbols) and computed (solid curve) fatigue response of epoxy. The experimental results are taken from [1].

fracture toughness $G_{Ic} = 88.97 \text{ J/m}^2$, and the cohesive strength $\sigma_{\max} = 35 \text{ MPa}$. The two parameters of the cohesive fatigue model (3) were taken to be $\alpha = 8 \text{ }\mu\text{m}$ and $\beta = 0.65$. As apparent in Fig. 2, the two-parameter cohesive model captures the entire fatigue failure response curve quite well, including the upper threshold at the higher crack growth rate regime, where the numerical results show the rapid acceleration of the fatigue crack for $\Delta K/K_{Ic} > 0.8$.

3. Cohesive modeling of wedge effect

The modeling of the wedge effect associated with the premature crack closure in the wake of the crack requires the incorporation in the model of a unilateral contact law characterized by the conditions of no interpenetration and no tension between the contacting bodies [3]. For a single DOF system, where a single node (contactor) is penetrating an object (obstacle), we define a distance function (g), referred to hereafter as *gap function*, as the signed distance between the contactor and the obstacle. We take g to be positive when the bodies are not in contact and negative when penetration occurs. The contact force p is taken to be negative for compression and positive for tension. The Hertz–Signorini–Moreau law of normal unilateral contact is expressed as [3]

$$g \geq 0, \quad p \leq 0, \quad gp = 0. \quad (6)$$

The first inequality expresses the condition of impenetrability, while the second one corresponds to the condition of no tension at the contact face. The third relation describes an energetic condition of zero work

between the gap-contact force pair. Let us also assume that no friction is present between the contact pair. These conditions can be implemented by a penalty method or by a Lagrange multiplier technique. As long as no wedge is present behind the crack tip, contact can occur only between the crack faces when the normal separation Δ_n becomes negative. To ensure no penetration between the crack faces in this situation, a penalty formulation is used. As shown in Fig. 1, for negative Δ_n , a large repulsive cohesive traction is produced to prevent inter-penetration. The slope of this branch of the traction-separation law can be deduced from (1) as $\sigma_{\max}/\Delta_{nc}(1 - \mathcal{S}_{\text{init}})$, which can be viewed as the stiffness of the penalty spring.

When a wedge of thickness Δ_n^* is inserted between the crack faces, the crack faces experience contact force whenever $\Delta_n - \Delta_n^* \leq 0$. This situation is depicted in Fig. 3. The use of the penalty method may lead to an excessive penalty force at the flanks of the crack giving rise to spurious increase in the crack driving force. Therefore, we adopt a Lagrange multiplier-based scheme, in which the contact forces can be estimated accurately. The contact algorithm between the crack flanks (denoted hereafter as “structure”) and the inserted wedge starts with the discretization of the wedge such that the wedge nodes coincide with the nodes on the structure when they are in contact (Fig. 4). In this particular geometry, the search procedure to find the contacting nodes/elements is highly simplified. The contact enforcement algorithm enforces contact exactly only at the nodes in a pointwise fashion, resulting in a link element method that can be viewed as a special case of the Lagrange multiplier technique (Fig. 4). Fictitious links are introduced between the contacting nodes, which can only transmit axial compressive forces when the gap between the wedge and beam nodes $\Delta_n - \Delta_n^*$ becomes zero or negative. When the gap is greater than zero, these link elements do not exist and the inequalities stated in (6) are thus satisfied.

The contact algorithm is implemented in a predictor–corrector fashion. At a given time step, the displacements at all structure and wedge nodes are calculated. If the gap between a node pair becomes negative, i.e., if there is a penetration between the wedge and structure, a link is formed at the point of contact. Let us assume that there are l node pairs at which penetration is detected and links are formed.

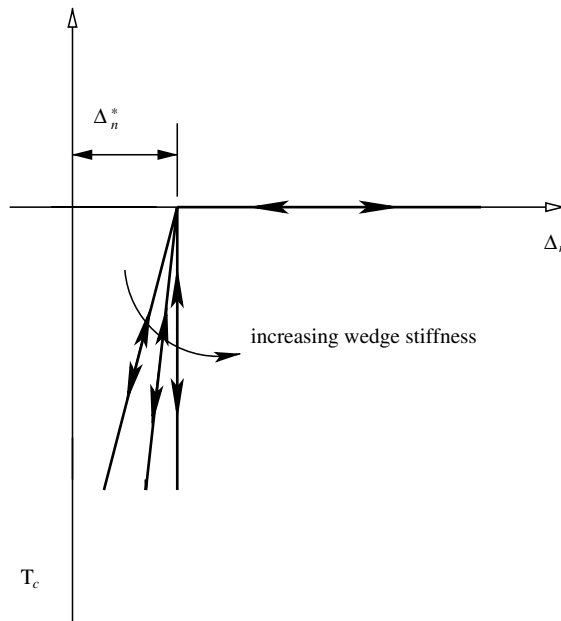


Fig. 3. Schematic representation of contact force T_c arising due to a wedge of thickness Δ_n^* inserted in the wake of the crack.

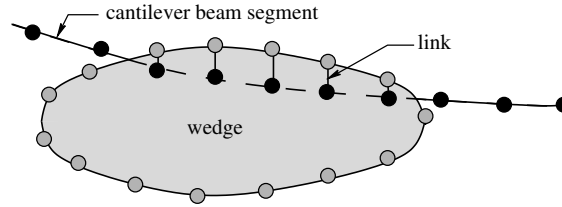


Fig. 4. Schematic of the wedge and the cracked portion of the DCB specimen in contact showing contacting nodes with link element between them.

Denoting the predicted displacements by a subscript p and the corrected ones by c , the displacement corrections ΔU are expressed as

$$\begin{aligned}\Delta U_i^b &= (u_p^b)_i - (u_c^b)_i, \\ \Delta U_i^w &= (u_p^w)_i - (u_c^w)_i \quad i = 1, \dots, l,\end{aligned}\quad (7)$$

where the superscript b and w denote the structure and wedge, respectively. Noting that for compatibility $(u_c^b)_i = (u_c^w)_i$, and denoting the penetration at the i th link by p_i , we arrive at

$$\Delta U_i^b - \Delta U_i^w = p_i. \quad (8)$$

The link force acting on the beam and the wedge can be written as

$$\begin{aligned}F_i^b &= K_{ij}^b \Delta U_j^b, \\ F_i^w &= K_{ij}^w \Delta U_j^w \quad i = 1, \dots, l, \quad j = 1, \dots, l,\end{aligned}\quad (9)$$

where \mathbf{K}^b and \mathbf{K}^w are the partitions of the stiffness matrices of the beam and wedge corresponding to the contacting nodes only. Equilibrium of the link forces dictates that

$$F_i^b + F_i^w = 0. \quad (10)$$

Substituting (9) into (10) and using the in matrix notation, we obtain

$$\mathbf{K}^b \Delta \mathbf{U}^b + \mathbf{K}^w \Delta \mathbf{U}^w = \mathbf{0}. \quad (11)$$

Making use of (8), the displacement correction for the structure $\Delta \mathbf{U}^b$ is expressed as

$$\Delta \mathbf{U}^b = (\mathbf{K}^b + \mathbf{K}^w)^{-1} \mathbf{K}^w \mathbf{p}. \quad (12)$$

Several simplifications of (12) are possible at this point. If the wedge is assumed to be a series of springs with equal stiffness W , (12) can be simplified to

$$\Delta \mathbf{U}^b = W(\mathbf{K}^b + I\mathbf{W})^{-1} \mathbf{p}. \quad (13)$$

Also, if the trace of the structure stiffness matrix $\text{Tr}(\mathbf{K}^b)$ is much smaller than that of the wedge, the wedge behaves rigidly and we find

$$\Delta \mathbf{U}^b \approx \mathbf{p},$$

i.e., the displacement correction for the structure becomes the penetration at contacting nodes.

The model is incorporated in the fatigue cohesive volumetric finite element (CVFE) code noting that the wedge is infiltrated only after a cohesive element fails completely thus giving rise to new crack faces. Furthermore, it is assumed that the wedge is inserted only at the peak stress regardless of its thickness Δ_n^* . The thickness is specified at each Gauss point of the failed cohesive elements which come into contact with the wedge. Hence, wedge contact is detected at a Gauss point if the normal opening Δ_n becomes less than or

equal to Δ_n^* with the predicted displacements at these nodes. The penetration vector \mathbf{p} is calculated based on these predicted displacements, and the displacement corrections $\Delta \mathbf{U}$ are found through the contact algorithm.

4. Results and discussion

In this section, we discuss the effect of the wedge-induced crack closure on the fatigue crack growth. In all the simulations presented hereafter, the fatigue parameters α and β are taken to be $8 \mu\text{m}$ and 0.3 , respectively. The material properties are those of epoxy and are listed in Section 2. The simulations are performed on a double cantilever beam of thickness 1 mm , length 40 mm and unit width with an initial crack length of 10 mm . In all cases, the beam is subjected to a cyclic load with a maximum amplitude of 250 N applied at the tip of the cantilever unless noted otherwise. The resulting crack propagation is thus unstable. For the geometry of the beam and this particular loading, the ratio of the initial stress intensity factor to the critical one is 0.5 and the stress intensity factor reaches its critical value when the crack extends by 10 mm . The length of the cohesive elements is taken to be 0.1 mm taking the spatial convergence criterion into account, i.e., the need to discretize the active cohesive zone with at least 4 cohesive elements at all times [12]. In all simulations, the wedge width is equal to that of the beam and the wedge is assumed to be rigid unless noted otherwise. The load ratio R is taken to be 0 unless otherwise noted.

4.1. Fatigue crack retardation by an infiltrated wedge

The characteristic effect of an inserted wedge on the crack propagation is shown in Fig. 5. The wedge is infiltrated after the crack has been extended by 1 mm and is assumed to fill the crack wake completely. The crack then advances past the wedge, but the wedge remains fixed at the inserted position. It is also assumed that the wedge has reached its fully cured state. In an adhesive injection setting, this would imply that loading be interrupted while the curing takes place. The thickness of the inserted wedges, Δ_n^* , is expressed as a fraction of the critical cohesive displacement jump Δ_{nc} . It can be thought that the different thicknesses result from the infiltration of the wedge at different applied stress levels in the loading cycle, which is designated by infiltration stress level (ISL) by some authors [17,19–21]. We prefer to specify the wedge thickness in this

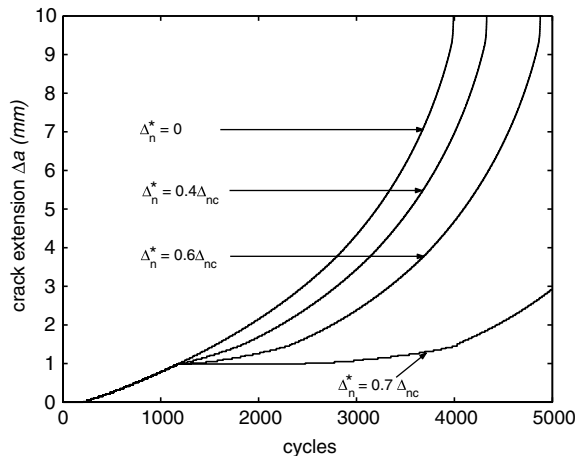


Fig. 5. Crack closure due to a wedge of varying thickness inserted after the crack has propagated by 1 mm .

study, as it directly relates to our simulations. We also assume here that the wedges are of uniform thickness.

Fig. 5 depicts the fatigue crack propagation behavior against the number of cycles for different thicknesses of the inserted wedge: $\Delta_n^* = 0.0, 0.4, 0.6,$ and $0.7\Delta_{nc}$. The static crack propagation behavior is observed for all the cases when the crack extension reaches 10 mm, length at which the stress intensity factor becomes critical and corresponding crack propagation curves become vertical. As apparent in Fig. 5, the crack propagation with inserted wedge exhibits three distinct regimes. Initially, all the curves follow the control case showing fatigue crack propagation in the absence of any retardation mechanism. After the wedge is inserted, there is an incubation period with no crack propagation observed for a while. The duration of the incubation period depends on the thickness of the wedge and is greater for higher values of Δ_n^* . Due to the inserted wedge, the crack closure is affected: the crack flanks cannot close fully at the wake during unloading thus reducing the effective stress intensity factor range ΔK_{eff} . As the thickness of the wedge increases, ΔK_{eff} decreases leading to an increased retardation. If ΔK_{eff} goes below the lower threshold value of the fatigue crack propagation, the crack can be arrested completely [2]. Finally, in the third regime, the fatigue crack resumes its propagation. Note that the rate of propagation is also influenced by Δ_n^* : it reduces with the increasing value of the wedge thickness. As the crack advances, it leaves the wedge in its wake at an increasing distance from the crack tip, thereby reducing the shielding effect on the crack tip. This fact is manifested by the gradual increase of the crack propagation rate in the third regime. These three distinct crack propagation regimes have been observed experimentally by Ur-Rehman and Thomason [23] for low-alloy steel with different wedge materials. The enhanced retardation of crack growth with increasing ISL (hence wedge thickness) is also consistent with other experimental [17] and theoretical observations [18].

Ur-Rehman and co-workers [23] also found that another key factor in fatigue crack retardation is the distance of the wedge from the crack tip which is also verified in [18] through a simple theoretical model based on weight function computations of the effect of the wedge present behind the crack tip. This fact is illustrated in Fig. 6. The wedges are inserted at different distances behind the crack tip when the crack has been extended by 2 mm and the thickness of wedge is kept constant at $0.7\Delta_{nc}$ while the wedge length is fixed at 1 mm for all the test cases. As apparent from the figure, more crack retardation is obtained for decreasing distance to the crack tip. As discussed before, the shielding effect of the wedge is reduced (i.e., the

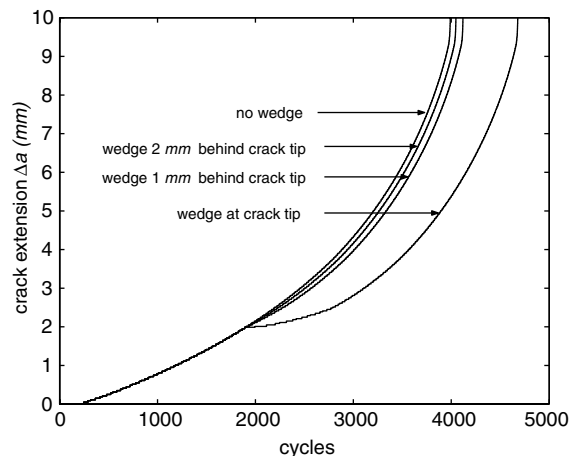
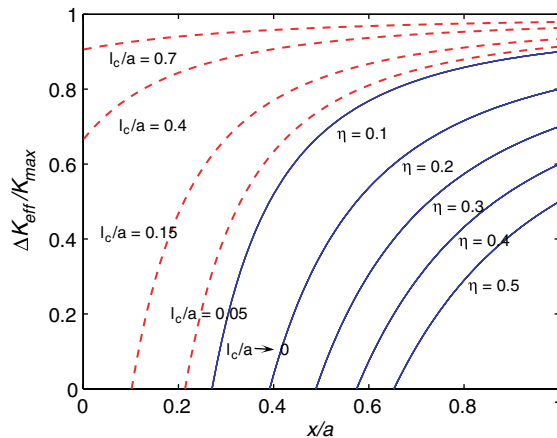


Fig. 6. Effect of the wedge infiltration at different distances behind the crack tip when the crack extension reaches $\Delta a = 2$ mm ($\Delta_n^* = 0.7\Delta_{nc}$).

effective stress intensity factor is increased) as the distance between the crack tip and the leading edge of the wedge increases. It has also been observed in our simulations that the length of the wedge does not play any role in the crack retardation, as it does not contribute towards reducing the crack driving force at the crack tip.

It should be noted here that the cohesive model of crack propagation adopted in the present study gets around the need for an explicit definition of the stress intensity factor. However, as it is usually done in the literature, we quantify the crack closure effect in terms of a reduction in the effective stress intensity factor. By analogy to the singular crack DCB model, a cohesive zone based DCB model can be constructed which further illustrates the effect of wedge insertion in the wake of the crack and also relates the “equivalent” stress intensity factor to the cohesive zone modeling for the particular specimen configuration. The details of the theoretical model, which relies on the classical solution of a beam on an elastic foundation, are given in [Appendix A](#). Let us respectively denote by a , l_c and x the crack length, cohesive zone length and distance between the wedge tip and the crack tip. Also, let P_{\max} and P^* respectively denote the maximum applied load and the load level at which the crack faces just touch the wedge tip. In a singular crack model of the DCB specimen (for which $l_c/a \rightarrow 0$), the ratio P^*/P_{\max} relates directly to the stress intensity factor ratio K^*/K_{\max} . In other words, $(P_{\max} - P^*)/P_{\max}$ is proportional to $\Delta K_{\text{eff}}/K_{\max}$. Assuming that similar relation holds in the presence of a cohesive zone, we plot in [Fig. 7](#) $\Delta K_{\text{eff}}/K_{\max}$ vs. x/a for various values of the wedge thickness $\eta = \Delta_n^*/2\delta_{\max}$ (with $l_c/a \rightarrow 0$, solid curves) and cohesive zone length (with $\eta = 0.1$, dashed curves). Here, δ_{\max} denotes the maximum deflection of the end of the beam (i.e., for $P = P_{\max}$). As apparent in [Fig. 7](#), as the wedge thickness increases (i.e., as η increases, solid curves), the crack closure effect it introduces becomes more prominent (i.e., ΔK_{eff} decreases) for a given insertion depth x . Note the rapid decrease of $\Delta K_{\text{eff}}/K_{\max}$ as the wedge is introduced closer to the crack tip, as described previously in [Fig. 6](#), especially for thinner wedges. The presence of the cohesive zone (dashed curves) does not affect these observations. In the limiting case ($l_c \rightarrow 0$), we recover the singular crack model (solid curve). As the size of the cohesive zone increases, the crack closure effect decreases due to an increased opening of the crack faces. It should be noted however that, in these computations, the trailing edge of the cohesive zone constitutes the farthest insertion point of the wedge, even if the corresponding opening displacement ($=\Delta_{\text{nc}}$) exceeds Δ_n^* , as it is the case for large values of l_c/a .



[Fig. 7](#). Effect of the distance x of a rigid wedge from the crack tip on the onset of crack closure, expressed in terms of $\Delta K_{\text{eff}}/K_{\max}$. The solid curves correspond to the singular limit ($l_c/a \rightarrow 0$) for various values of the wedge thickness ($\eta = \Delta_n^*/2\delta_{\max}$), while the dashed curves correspond to various values of l_c/a for $\eta = 0.1$.

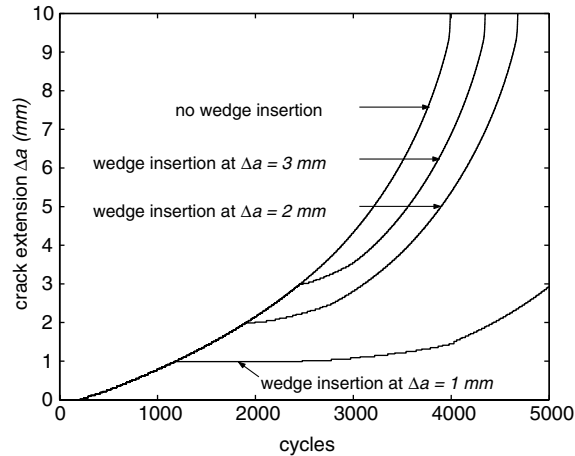


Fig. 8. Effect of a 1 mm long wedge inserted behind the crack tip after the crack has extended by 1, 2, 3 and 4 mm ($A_n^* = 0.7A_{nc}$) for a DCB specimen under cyclic loading with a constant load amplitude.

Next, we study the effect of a 1 mm long wedge inserted right at the crack tip when the crack has advanced by 1, 2 and 3 mm. It can be seen from Fig. 8 that, the sooner the wedge is inserted, the more effective the retardation mechanism becomes. Since the crack driving force at the crack tip increases with crack advance and gives rise to a higher stress intensity factor range, the wedge insertion is more effective in retarding the crack when the prevailing stress intensity factor is lower. This observation is further reinforced by the results presented in Fig. 9 where the same situation is studied, but instead of the constant load applied earlier, a cyclic displacement with a constant amplitude of 0.65 mm is applied, which gives rise to an initial stress intensity factor 5% higher than the critical one. The crack starts propagating in a steady fashion, but, as the crack length increases, the stress intensity factor is reduced for this type of loading. The crack

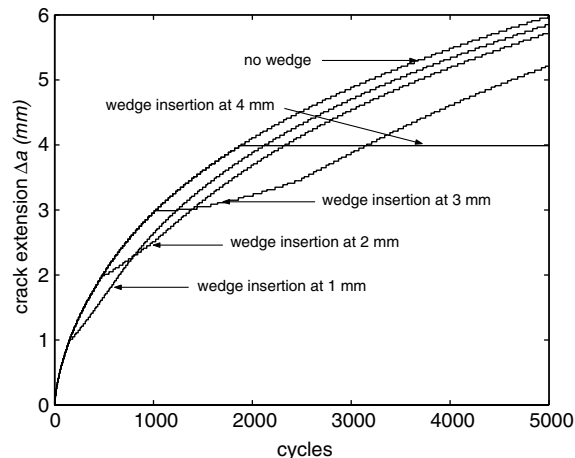


Fig. 9. Effect of a 1 mm long wedge inserted behind the crack tip after the crack has extended by 1, 2, 3 and 4 mm. The thickness of the wedge for all the cases is $0.7A_{nc}$ and the DCB specimen is subjected to a cyclic loading with a constant displacement amplitude.

propagation becomes sub-critical (i.e., is expected to stop under quasi-static loading conditions but can propagate under cyclic loading) after the crack extends by 0.2 mm. The wedge becomes more effective in retarding the crack for this type of loading if inserted late, allowing the crack to propagate more and thereby reducing the stress intensity factor further. For a crack advance $\Delta a = 4$ mm, the crack gets actually arrested.

4.2. Continuous delivery of crack filling material

All the observations made in the previous section, i.e., the effect of the wedge thickness, the distance of the wedge from the crack tip and the wedge insertion schemes, point to the fact that the inserted wedge shields the crack tip by reducing the effective stress intensity factor, thus retarding the crack growth. It can also be concluded that the crack filling mechanism by which the advancing crack tip can be closely followed by a wedge will produce the best result for the retardation of fatigue cracks assuming other factors (such as the wetting of the crack faces and through-thickness penetration) to be constant. So the biggest challenge of this type of crack-retarding mechanism is the design of an effective mechanism which can deliver the new material in the wake of the crack continuously. The continuous delivery of crack wake filling material is achieved in the case of the self-healing material described in the introduction [2,25]. The solidification of the delivered substance depends on the healing chemistry of the material. For the present study, we will assume that the crack is rested intermittently so that the polymerization of the healing agent is complete, and the wedge can be modeled as a rigid body. We also assume that the thickness of the deposited wedge is uniform throughout the wedge. Referring back to Fig. 6, it can be stated that the continuous delivery of the crack filling material upto the crack tip is the best method to slow down crack advance regardless of the loading environment for a given wedge thickness.

Fig. 10 depicts the crack propagation behavior in the presence of a continuously delivered wedge of varying thicknesses. It can be observed that the three distinct crack propagation regimes observed earlier are absent for these cases. The propagation of the fatigue crack starts to slow down from the very beginning and the crack growth rate decreases as the wedge thickness is increased, as observed experimentally in [2]. As the thickness of the wedge is increased, the crack actually gets arrested as the crack driving force at the crack tip reaches a threshold beyond which no crack propagation is possible [12].

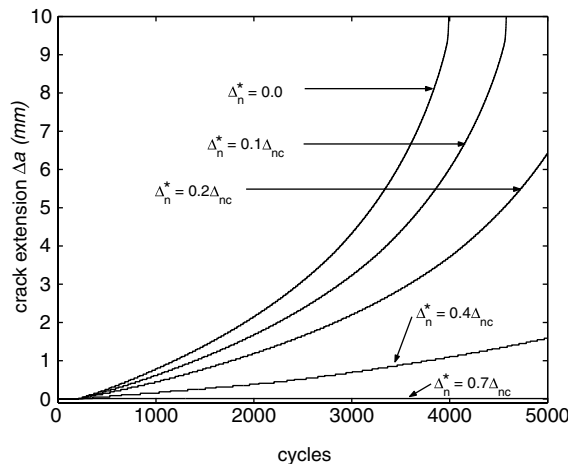


Fig. 10. Continuously inserted wedge: effect of wedge thickness on the fatigue crack propagation.

4.3. Effect of applied loading on fatigue crack retardation

As the applied load level is increased, the stress intensity factor range ΔK increases. The crack then experiences an increased driving force leading to an increased rate of propagation. A direct comparison of the effect of the inserted wedge thus becomes difficult. For that reason, Fig. 11 presents the crack extension vs. number of cycles both for the case with no wedge as well as with a continuously injected wedge of thickness $0.7A_{nc}$ at $\Delta a = 1$ mm for three different applied cyclic load levels. The applied load amplitudes are 200, 250 and 350 N, which correspond to initial values of $\Delta K/K_{Ic}$ of 0.4, 0.5 and 0.7, respectively. R is taken to be 0 for all cases. As expected, the crack propagation rate is higher for higher values of applied tractions. But we also observe that crack retardation due to the wedge also reduces substantially with higher loading. As the geometry of the infiltrated wedge is constant for all these cases, it modifies K_{min} by the same magnitude. Hence its contribution towards reducing the stress intensity factor range, ΔK , remains the same in all cases. But higher applied loadings give rise to higher values of K_{max} , hence higher ΔK so that the effective stress intensity factor range experienced by the crack tip increases with an increase of the applied loading. Moreover, as the loading increases, the crack also starts propagating early at a faster rate, giving rise to a further increase in the effective stress intensity factor range.

We also study the effect of the load ratio R in this context. The value of R is varied by changing the minimum value of the applied load keeping the maximum value constant for all cases. The maximum amplitude of the applied loading is 250 N on each arm of the DCB specimen, the thickness of the wedge is chosen as $0.4A_{nc}$ and it is assumed to span the whole wake of the crack. Three values of R are considered: $R = 0.2, 0.5$ and 0.7 . As shown in Fig. 12, R plays two key roles on the fatigue failure of the DCB specimen. In the absence of a wedge (solid curves), it strongly affects the fatigue crack propagation rate through the value of the intercept C of the Paris curve (inset of Fig. 12). Furthermore, the load ratio R affects the extent of the crack closure effect introduced by the wedge (dashed curves), thereby modifying the retardation achieved. As the load ratio increases, the lower value of the loading cycle increases also. Since the wedge thickness is constant for all these cases, the portion of the loading cycle at which the crack face and the wedge are in contact also goes down with increasing R . As R increases, for some threshold value, the crack face actually loses contact with the wedge rendering the crack closure mechanism ineffective. For $R = 0.7$, although the crack propagation rate is much lower both for the control case and the case with infiltrated wedge, there is almost no difference in crack propagation rate for these two cases.

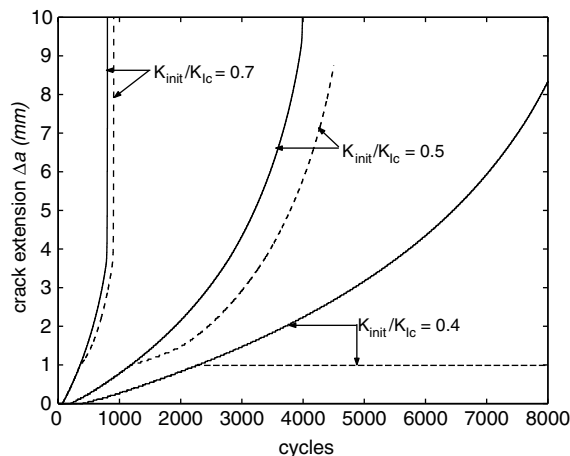


Fig. 11. Effect of initial stress intensity factor on the evolution of the crack advance ($A_n^* = 0.70A_{nc}$) for a wedge inserted at $\Delta a = 1$ mm. The solid and dashed curves respectively correspond to the solution in the absence and presence of a wedge.

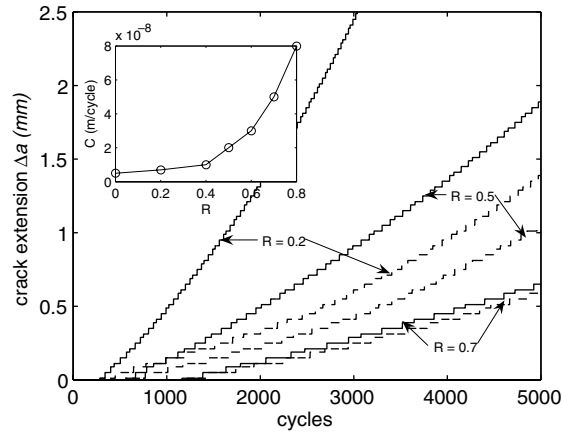


Fig. 12. Effect of the loading ratio R on the evolution of crack advance. The wedge is continuously inserted and is of thickness $0.4A_{nc}$. The solid and dashed curves denote the fatigue response without and with the wedge, respectively. The inset shows the R -dependence of the intercept C of the Paris fatigue curve in the absence of a wedge.

4.4. Effect of wedge stiffness

We now present the effect of the inserted wedge stiffness on the fatigue crack retardation behavior. In their study, Ur-Rehman and Thomason [23] assumed the wedge to be rigid. They argued that a low-strength elastic wedge will behave as a rigid body due to small deformation and large plastic constraint. Shin and Cai [18] subsequently presented a model taking the stiffness of the wedge into account. However they assumed the crack flank to be rigid, compared to the low stiffness of the inserted polymeric wedges.

As we are investigating the polymeric wedges inserted in the wake of a crack in a polymeric specimen, we need to account for the compliance of both the crack flanks and the wedge using the contact model described in Section 3. For this particular study, we use the simplified version of (12) where the wedge is assumed to be constituted of a series of springs of stiffness W (see (13)). The value of W is chosen to be a fraction of the transverse stiffness K_{beam} of the DCB specimen, i.e., of the diagonal term of the global beam stiffness matrix corresponding to the translational degree of freedom. Note that, since the beam has been discretized in elements of equal lengths, all the diagonal terms corresponding to either translational or rotational DOF are equal to each other, except at the boundary nodes. For an arbitrary node along the beam, the transverse stiffness is K_{beam} . In Fig. 13, we present the effect of the stiffness of the wedge (springs) W on the evolution of crack advance. As expected, for very low values of the wedge stiffness, the crack retardation is almost negligible. As the wedge stiffness is increased, initial retardation is increased whereas subsequent crack growth rate is almost similar to the case with no inserted wedge. This result can be explained by the fact that, as the crack moves ahead, the effect of the inserted wedge on the reduction of crack closure decreases significantly and ultimately becomes zero. Also, the increased compliance of the inserted wedge allows the crack flanks to come closer to each other thus reducing the effectiveness of the wedge in retarding the crack growth. Finally, when the wedge behaves as a rigid body, it is most effective in influencing crack closure and thus fatigue crack growth. This fact is clearly visible in Fig. 13: the rigid wedge arrests the crack, and when the crack starts to grow again, the rate of growth is significantly lower than in other cases.

4.5. Change in compliance of DCB specimen

We finally turn our attention to the change in compliance of the DCB specimen due to fatigue crack growth and retardation by investigating the effect of an inserted wedge of finite length and constant

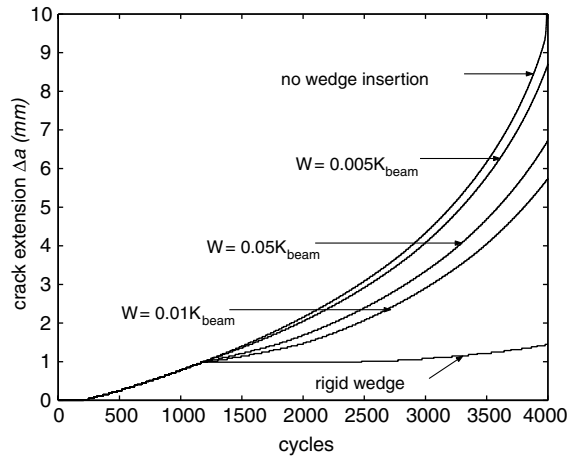


Fig. 13. Evolution of the crack advance with varying stiffness W of a wedge of thickness $0.7A_{nc}$ inserted at $\Delta a = 1$ mm. The translational stiffness of the beam is denoted by K_{beam} .

thickness on the evolution of the load vs. deflection curve. The peak value of the applied load is taken to be 250 N with $R = 0$, and the wedge thickness is $0.7A_{nc}$. The wedge is inserted when the crack extension reaches 1 mm. The load point displacement is measured for the DCB specimen and the applied traction is plotted against it in Fig. 14(b) for a few chosen loading cycles labeled on the crack advance vs. cycle curve in Fig. 14(a). The slope of these curves corresponds to the inverse of the compliance of the structure at a given loading cycle. Note that each curve contains the loading as well as the unloading part of a loading cycle, and the curves are arbitrarily shifted along x-axis for clarity.

As mentioned in Section 4.1, the crack propagation comprises of three distinct regimes. At the very beginning (cycle 1 in Fig. 14), the crack does not propagate at all as damage has not had the chance to accumulate yet in the cohesive zone ahead of the initial crack tip. The specimen has thus the lowest compliance among all cycles. Subsequently, as enough damage accumulates in the cohesive zone, the crack starts extending in a sub-critical manner giving rise to the first regime of crack propagation. The load–displacement curve for the 1000th cycle shows an increase in compliance due to the extension of the original crack. After about 1000 cycles (and a 1 mm crack extension), the crack enters the second regime of propagation: the incubation period. In this regime, the effective stress intensity factor range at the crack tip is lowered by the wedge insertion yielding a temporary crack arrest. The rigid wedge bears the compressive load during the unloading part of the loading cycle and the compliance is decreased, as shown by the curve associated with the 2000th cycle. The compliance is still slightly higher than that of the original DCB specimen (cycle 1), denoting the fact that the crack faces lose contact with the wedge during part of the loading cycle, but the resultant ΔK_{eff} is not sufficient to drive the crack. After about 3000 cycles, the crack tip region accumulates enough damage to nucleate fatigue crack growth again, but at a lower rate than the original one.

The load–displacement curve for the 4000th cycle is bi-linear, with the lower portion still retaining the previous compliance due to the crack closure, but the upper portion is more compliant due to the advancing crack in the loading part of the cycle. In subsequent cycles, the “knee” of the curves (denoted by a broken line in Fig. 14(b)) goes towards lower applied load levels; the slope of the lower curve remains the same, but the upper portion becomes more compliant with the passing cycles. As the advancing crack leaves the wedge further down its wake, the crack closure effect diminishes continually, as apparent by the lowering of the “knee”. At about cycle 5500, the “knee” vanishes completely indicating the absence of the crack closure altogether, and the fatigue crack regains its original propagation rate. This evolution of the compliance has also been reported in [17, Fig. 3] and [1, Fig. 7.20].

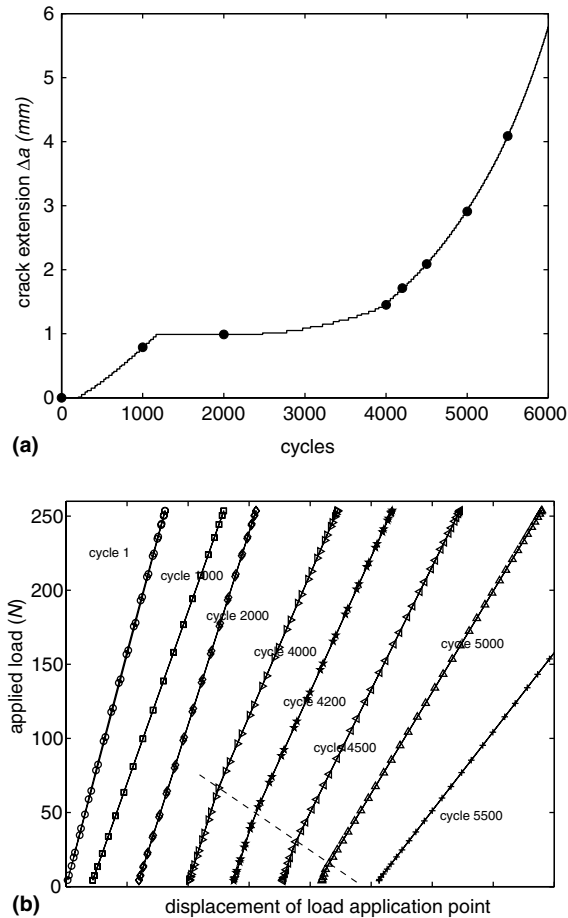


Fig. 14. Evolution of reaction due to applied loading with crack extension: (a) crack extension vs. cycles of loading with the cycles at which the load–reaction curves are extracted shown with circles; (b) load–reaction response, with the curves shifted arbitrarily along the x -axis for clarity.

5. Conclusions

We have presented the formulation and implementation of a cohesive model used to capture the retardation of fatigue crack growth associated with the insertion of a wedge in the wake of an advancing crack. The approach relies on the combination of a two-parameter cohesive model used to capture the progressive degradation of the cohesive failure properties of polymers with a crack closure scheme that captures the interaction between the newly created crack faces and the wedge. The model has been implemented in a cohesive finite element framework using a predictor–corrector scheme combined with a link-based approach to capture the contact between the crack faces and the wedge.

The effect of various loading and geometric parameters has been studied systematically and the numerical results have been compared with experimental observations whenever possible, showing very good qualitative agreement even though many of these experiments have been performed on metals. This somewhat surprising result can be explained by the fact that, in these experiments, crack retardation was primarily promoted by the inserted wedge, not by the plastic behavior of the material. This agreement is however an indication of the flexibility of the proposed scheme.

Simulations have shown that the major factor for fatigue crack retardation is the proximity of the wedge with the crack tip and the thickness of the wedge. Also, the wedge is more effective when it is inserted at lower stress intensity factor level. The key motivation for this study was the modeling of the fatigue response of a self-healing polymer-based material. Simulations performed with the cohesive model have shown that, by delivering the wedging material in the immediate vicinity of the advancing crack front, this system provides the most efficient delivery scheme.

Acknowledgements

The authors gratefully acknowledge the support provided by the AFOSR Aerospace and Materials Science Directorate (Grant # F49620-02-1-0080). They also wish to thank Dr. Eric Brown and Prof. Nancy Sottos for helpful discussions.

Appendix A. Beam theory analysis of onset of crack closure

The cohesive zone ahead of the crack tip can be thought of a beam of length l_c (cohesive zone length) on an elastic foundation with a stiffness of k_f . Although k_f varies within the cohesive zone for the bi-linear cohesive law described in Section 2, we take k_f to be constant in this analysis. The crack length is denoted by a . For the problem of an elastic beam on a partial elastic foundation shown in Fig. 15, the displacement δ at a distance x from the crack tip due to an applied load of P can be written as

$$\delta = \Delta + \theta x + \frac{Pax^2}{2EI} - \frac{Px^3}{6EI}, \quad (\text{A.1})$$

where the displacement at the crack tip (i.e., at the trailing edge of the cohesive zone) Δ is given by

$$\Delta = -\frac{P(e^{-2\bar{\beta}} - ae^{-2\bar{\beta}}\bar{\beta} + 4a(\cos\bar{\beta})^2\bar{\beta} + 4\cos\bar{\beta}\sin\bar{\beta} - 2a\bar{\beta} - a\bar{\beta}e^{2\bar{\beta}} - e^{2\bar{\beta}})}{2EI(e^{-2\bar{\beta}} + 4(\cos\bar{\beta})^2 + 2 + e^{2\bar{\beta}})\bar{\beta}^3} = -\frac{P\mathcal{N}_1}{2EI\mathcal{D}\bar{\beta}^3}, \quad (\text{A.2})$$

and the slope at the crack tip is written as

$$\theta = \frac{P(e^{-2\bar{\beta}} - 2ae^{-2\bar{\beta}}\bar{\beta} - 4(\cos\bar{\beta})^2 + 8a\bar{\beta}\sin\bar{\beta}\cos\bar{\beta} + 2 + e^{2\bar{\beta}} + 2a\bar{\beta}e^{2\bar{\beta}})}{2EI(e^{-2\bar{\beta}} + 4(\cos\bar{\beta})^2 + 2 + e^{2\bar{\beta}})\bar{\beta}^2} = \frac{P\mathcal{N}_2}{2EI\mathcal{D}\bar{\beta}^2}, \quad (\text{A.3})$$

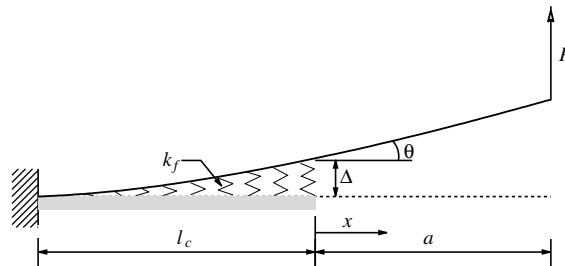


Fig. 15. Schematic of a cantilever beam partially on an elastic foundation of stiffness k_f and subjected to a point load P at the tip. l_c and a respectively denote the cohesive zone and crack lengths.

with

$$\beta = (k_r/4EI)^{0.25} \quad \text{and} \quad \bar{\beta} = \beta l_c.$$

Note that, when $l_c \rightarrow 0$, Δ and θ also tends to zero and (A.1) represents the equation of the deflected shape of a cantilever beam with a point load at one end.

Let us rewrite (A.1) in the following form:

$$\delta = \delta_{\text{tip}} \left[-\frac{1.5\mathcal{N}_1}{\mathcal{D}\bar{\beta}^3} (l_c/a)^3 + \frac{1.5\mathcal{N}_2}{\mathcal{D}\bar{\beta}^2} (l_c/a)^2 (x/a) + 1.5(x/a)^2 - 0.5(x/a)^3 \right], \quad (\text{A.4})$$

with δ_{tip} denoting the displacement at the tip due to an applied load of P

$$\delta_{\text{tip}} = \frac{Pa^3}{3EI}.$$

Denote the wedge thickness by Δ_n^* and assume that a load of P^* (and corresponding SIF K^*) is required to obtain $\delta = \Delta_n^*/2$ at a distance x from the crack tip. Also assume that the maximum loading on the specimen is P_{max} and corresponding tip displacement is δ_{tipmax} so that

$$\frac{P^*}{P_{\text{max}}} = \eta \left[\frac{1}{-\frac{1.5\mathcal{N}_1}{\mathcal{D}\bar{\beta}^3} (l_c/a)^3 + \frac{1.5\mathcal{N}_2}{\mathcal{D}\bar{\beta}^2} (l_c/a)^2 (x/a) + 1.5(x/a)^2 - 0.5(x/a)^3} \right], \quad (\text{A.5})$$

where

$$\eta = \frac{\Delta_n^*}{2\delta_{\text{tipmax}}}.$$

Assuming the stress intensity factor is linearly related with the applied loading as in the case of singular crack without the cohesive zone, (A.5) can be expressed as

$$\frac{\Delta K_{\text{eff}}}{K_{\text{max}}} = \frac{K_{\text{max}} - K^*}{K_{\text{max}}} = 1 - \frac{K^*}{K_{\text{max}}} \simeq 1 - \frac{P^*}{P_{\text{max}}}. \quad (\text{A.6})$$

References

- [1] Brown EN. Fracture and fatigue of a self-healing polymer composite material. PhD thesis, University of Illinois at Urbana-Champaign, 2003.
- [2] Brown EN, White SR, Sottos NR. Retardation and repair of fatigue cracks in a microcapsule toughened epoxy composite—Part II: In situ self-healing. *Comp Science & Techn*, to appear.
- [3] Curnier A. Unilateral contact: mechanical modelling. In: Wriggers P, Panagiotopoulos P, editors. *New developments in contact problems*. New York: SpringerWien; 1999. p. 1–54.
- [4] de-Andres A, Pérez JL, Ortiz M. Elastoplastic finite element analysis of three-dimensional fatigue crack growth in aluminium shafts subjected to axial loading. *Int J Solids Struct* 1999;36:2231–58.
- [5] Deshpande VS, Needleman A, Van der Giessen E. A discrete dislocation analysis of near-threshold fatigue crack growth. *Acta Mater* 2001;49(16):3189–203.
- [6] Deshpande VS, Needleman A, Van der Giessen E. Discrete dislocation modeling of fatigue crack propagation. *Acta Mater* 2002;50(4):831–46.
- [7] Elber W. Fatigue crack closure under cyclic tension. *Engng Fract Mech* 1970;2:37–45.
- [8] Endo K, Okada T, Komai K, Kiota M. Fatigue-crack propagation of steel in oil. *Bull JSME* 1972;15:1316–23.
- [9] Haliday MD, Beevers CJ. Non-closure of cracks and fatigue-crack growth in β -heated treated Ti–6Al–4V. *Int J Fract* 1979;15:R27–30.
- [10] Hornbogen E. Martensitic transformation at a propagating crack. *Acta Metall* 1978;26:147–52.

- [11] Kitagawa H, Toyohiro S, Ikeda I. A new method of arresting fatigue crack growth by artificial wedge. Proceedings of international conference on fracture mechanics in engineering applications, National Aeronautical Laboratory, Bangalore, India. Sijthoff and Noordhoff; 1979. p. 281–92.
- [12] Maiti S, Geubelle PH. A cohesive model for fatigue failure of polymers. *Engng Fract Mech* 2005;72(5):691–708.
- [13] Nguyen O, Repetto EA, Ortiz M, Radovitzky RA. A cohesive model of fatigue crack growth. *Int J Fract* 2001;110:351–69.
- [14] Ritchie RO. Mechanisms of fatigue crack propagation in metals, ceramics and composites: role of crack tip shielding. *Mater Sci Engng* 1988;A103:15–28.
- [15] Ritchie RO, Suresh S. A geometric model for fatigue crack closure induced by fracture surface roughness. *Met Trans* 1982;13A:937–40.
- [16] Roe KL, Siegmund T. An irreversible cohesive zone model for interface fatigue crack growth simulation. *Engng Fract Mech* 2003;70:209–32.
- [17] Sharp PK, Clayton JQ, Clark G. Retardation and repair of fatigue cracks by adhesive infiltration. *Fatigue Fract Engng Mater Struct* 1997;20(4):605–14.
- [18] Shin CS, Cai CQ. A model for evaluating the effect of fatigue crack repair by the infiltration method. *Fatigue Fract Engng Mater Struct* 2000;23:835–45.
- [19] Shin CS, Huang KC, Li RZ. Artificial retardation of fatigue crack growth by the infiltration of cracks by foreign materials. *Fatigue Fract Engng Mater Struct* 1998;21:835–46.
- [20] Shin CS, Wang CM, Song PS. Fatigue damage repair: a comparison of some possible methods. *Int J Fatigue* 1996;18(8):535–46.
- [21] Song PS, Hwang S, Shin CS. Effect of artificial closure materials on crack growth retardation. *Engng Fract Mech* 1998;60(1):47–58.
- [22] Suresh S, Zamiski GF, Ritchie RO. Oxide-induced crack closure: an explanation for near-threshold corrosion fatigue crack growth behavior. *Met Trans* 1981;12A:1435–43.
- [23] Ur-Rehman A, Thomason PF. The effect of artificial fatigue-crack closure on fatigue-crack growth. *Fatigue Fract Engng Mater Struct* 1993;16(10):1081–90.
- [24] Vecchio RS, Crompton JS, Hertzberg RW. Anomalous aspects of crack closure. *Int J Fract* 1986;31:R29–33.
- [25] White SR, Sottos NR, Moore J, Geubelle PH, Kessler M, Brown E, et al. Autonomic healing of polymer composites. *Nature* 2001;409:794–7.
- [26] Yang B, Mall S, Ravi-Chandar K. A cohesive zone model for fatigue crack growth in quasibrittle materials. *Int J Solids Struct* 2001;38:3927–44.
- [27] Yanyan W, Mingxu Z, Daqing F. A study of retarding fatigue crack growth using an artificial wedge. *Fatigue Fract Engng Mater Struct* 1993;16:363–76.